Stabilization of hydrodynamic flows by small viscosity variations

Rama Govindarajan,[1] Victor S. L'vov,[2] Itamar Procaccia,[2] and A. Sameen[3]

[1]*Fluid Dynamics Unit, Jawaharlal Nehru Centre for Advanced Scientific Research, Jakkur, Bangalore 560064, India*
[2]*Department of Chemical Physics, The Weizmann Institute of Science, Rehovot 76100, Israel*
[3]*Department of Aerospace Engineering, Indian Institute of Science, Bangalore 560012, India*

Motivated by the large effect of turbulent drag reduction by minute concentrations of polymers, we study the effects of a weakly space-dependent viscosity on the stability of hydrodynamic flows. In a recent paper [Phys. Rev. Lett. **87**, 174501, (2001)], we exposed the crucial role played by a localized region where the energy of fluctuations is produced by interactions with the mean flow (the "critical layer"). We showed that a layer of a weakly space-dependent viscosity placed near the critical layer can have a very large stabilizing effect on hydrodynamic fluctuations, retarding significantly the onset of turbulence. In this paper we extend these observations in two directions: first we show that the strong stabilization of the primary instability is also obtained when the viscosity profile is realistic (inferred from simulations of turbulent flows with a small concentration of polymers). Second, we analyze the secondary instability (around the time-dependent primary instability) and find similar strong stabilization. Since the secondary instability develops around a time-dependent solution and is three dimensional, this brings us closer to the turbulent case. We reiterate that the large effect is *not* due to a modified dissipation (as is assumed in some theories of drag reduction), but due to reduced energy intake from the mean flow to the fluctuations. We propose that similar physics act in turbulent drag reduction.

I. INTRODUCTION

This paper is motivated by the dramatic effects that are observed with the addition of small amounts of polymers to hydrodynamic flows. While interesting effects were discussed in the context of the transition to turbulence, vortex formation, and turbulent transport [1], the phenomenon that attracted the most attention was, for obvious reasons, the reduction of friction drag by up to 80% when very small concentrations of long-chain polymers were added to turbulent flows [2,3]. In spite of the fact that the phenomenon is robust and the effect huge, there exists no accepted theory that can claim a quantitative agreement with the experimental facts. Moreover, it appears that there is no mechanistic explanation. In the current theory that is due to de Gennes [4,5], one expects the Kolmogorov cascade to be terminated at scales larger than Kolmogorov scale, leading somehow to an increased buffer layer thickness and reduced drag, but how this happens and what is the fate of the turbulent energy is not being made clear.

In a recent paper [6], we proposed that the crucial issue is in the *production* of energy of hydrodynamic fluctuations by their interaction with the mean flow. For the sake of concreteness we examined a Poiseuille laminar flow and its loss of linear stability, and showed how small viscosity contrasts lead to an order of magnitude retardation in the onset of instability of "dangerous" disturbances. Specifically, we considered a flow in a channel of dimensionless width 2, in which there are two fluids: one fluid of viscosity μ_1 flows near the walls and the other fluid of viscosity μ_2 flows at the center, see Fig. 1. The viscosities differ slightly, for example, we considered (in dimensionless units) $\mu_2 = 1$ and $m = \mu_1/\mu_2 = 0.9$. The main ingredient of the calculation was that all the viscosity difference of 0.1 concentrated in a "mixed" layer of width 0.10. The motivation behind these numbers was the observation that the inferred effective viscosity in polymer drag reduction increases towards the center by about 30% over about a 1/3 of the half channel [7]. With our choice we have comparable viscosity gradients in the mixed layer.

In this model everything was explicitly calculatable. The main point of our analysis (see Sec. II for further details) was that there exists a position in the channel where the velocity of the mean flow is the same as the velocity of the most dangerous primary instability. Below we refer to the layer around this position as the "critical layer" [8]. If we placed the mixed layer in the vicinity of the critical layer, we got a giant effect of stabilization. Analyzing this phenomenon, we demonstrated that nothing special happened to the dissipation. Rather, it was the energy intake from the mean flow to the unstable mode that was dramatically reduced, giving rise to a large effect for a small cause. In this paper we extend these observations in two directions. In Sec. II, after review-
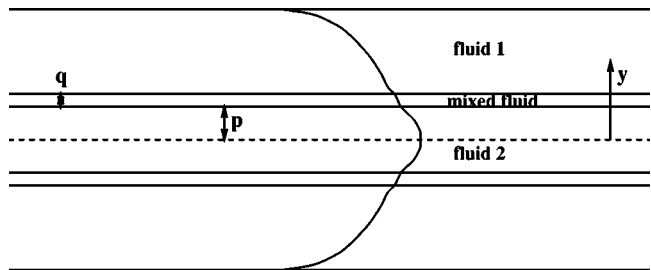

FIG. 1. Schematic of the flow, the fluid near the walls has a viscosity μ_1, and that flowing at the center is of viscosity μ_2. In the mixed layer (of width q), the viscosity varies gradually between μ_1 and μ_2. The parameter p controls the position of the mixed layer. For simplicity we neglect the down-stream growth in q.

ing the results of the simple model, we extend the analysis of the primary instability to a case in which the viscosity profile is that inferred from direct numerical simulations of turbulent channel flow of a dilute polymeric solution [7]. We will see that very similar effects are found. In other words, one does not need to put by hand the region of viscosity variation in the vicinity of the critical layer. When we have a continuous variation of the viscosity in the region near the wall, the effect is the same, since it is only crucial that there will be *some* space dependence of the viscosity in the critical layer, which is usually not too far from the wall.

A possible criticism of our results can be that the primary instability is still too far from typical turbulent fluctuations. This is, in particular, true since the most unstable primary modes are two-dimensional, whereas typical turbulent fluctuations are three-dimensional. For these reasons we present in Sec. III the analysis of the effect of small viscosity variations on the secondary instability, for which the most "dangerous" modes are three-dimensional. The tactics are similar to those taken for the primary instability. First we discuss the effects of a mixed layer put at the "right" place in the channel, and second we show that continuous viscosity profiles do exactly the same. We find again the giant effect of stabilization for relatively small viscosity variations, lending further support to our proposition that similar effects may very well play a crucial role in turbulent drag reduction. In Sec. IV we present concluding remarks and suggestions for the road ahead.

II. PRIMARY INSTABILITY OF POISEUILLE FLOW

It is well known that parallel Poiseuille flow loses linear stability at some threshold Reynolds number $\text{Re}=R_{th}$ (close to 5772). It is also well known that the instability is "convective," with the most unstable mode having a phase velocity c_p. Analytically it has the form

$$\hat{\phi}_p(x,y,t) = \frac{1}{2}\{\phi_p(y)\exp[ik_p(x-c_pt)]+\text{c.c.}\}\exp(\gamma_p t),$$

(1)

where c.c. stands for the complex conjugate, the subscript p stands for the primary instability, $\hat{\phi}(x,y,t)$ is the disturbance stream function, and $\phi(y)$ is the complex envelope of $\hat{\phi}(x,y,t)$. We have chosen x and y as the streamwise and wall-normal coordinates, respectively, k as the streamwise wavenumber of the disturbance and t as time. γ_p is the growth rate of the primary instability. What is not usually emphasized is that the main interactions leading to the loss of stability occur in a sharply defined region in the channel, i.e., at the critical layer whose distance from the wall is such that the phase velocity c is identical to the velocity of the mean flow somewhere within this layer. It is thus worthwhile to examine the effect on the stability of Poiseuille flow of a viscosity gradient placed in the vicinity of the critical layer. This will provide us with a very sharp understanding of the mechanism of the stabilization of the flow by viscosity variations. In the following subsection we will examine the case of continuous viscosity profiles.
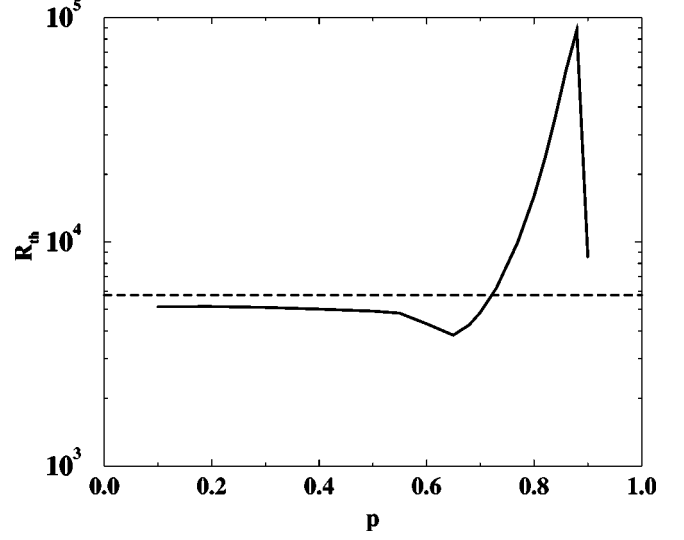

FIG. 2. The dependence of the threshold Reynolds number R_{th} on the position of the viscosity stratified layer for $m=0.9$. The dashed line pertains to the neat fluid. Note the huge increase in R_{th} within a small range. This occurs when the stratified layer overlaps the critical layer.

A. Mixed layer

A report of the results of this subsection was provided in Ref. [6]. We examine a channel flow of two fluids with different viscosities μ_1 and μ_2, see Fig. 1.

The observation that we want to focus on is shown in Fig. 2: the threshold Reynolds number for the loss of stability of the mode as in Eq. (1) depends crucially on the position of the mixed layer. When the latter hits the critical layer, the threshold Reynolds number for the loss of stability reaches as much as 88 000. In other words, one can increase the threshold of instability *for a given mode* 15 times, and by making the mixed layer thinner one can reach even higher threshold Reynolds values. In Ref. [6] we analyzed the physical origin of this huge sensitivity of the flow stability to the profile of the viscosity.

The stability of this flow is governed by the modified Orr-Sommerfeld equation [9]

$$ik_p[(D^2\phi_p-k_p^2\phi_p)(\bar{U}-c_p-i\gamma_p)-D^2\bar{U}\phi_p]$$

$$= \frac{1}{\text{Re}}[\mu D^4\phi_p+2D\mu D^3\phi_p+(D^2\mu-2k_p^2\mu)D^2\phi_p$$

$$-2k_p^2D\mu D\phi_p+(k_p^2D^2\mu+k_p^4\mu)\phi_p],$$

(2)

in which $\bar{U}(y)$ is the basic laminar velocity, the operator D stands for differentiation with respect to the normal coordinate y, and μ is a function of y. The boundary conditions are $\phi_p(\pm1)=D\phi_p(\pm1)=0$. All quantities have been nondimensionalized using the half-width H of the channel and the centerline velocity U_0 as the length and velocity scales, respectively. The Reynolds number is defined as $\text{Re}\equiv\rho U_0 H/\mu_2$, where ρ is the density (equal for the two fluids). The primes stand for derivative with respect to y. At y
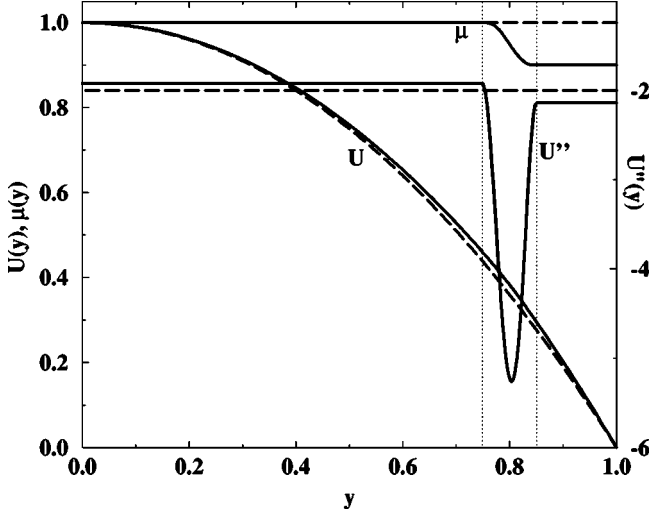
FIG. 3. Profiles of the normalized viscosity $\mu(y)$ and normalized velocity $\bar{U}(y)$ and the second derivative $D^2\bar{U}(y)$ for $m=0.9$ (solid lines) and $m=1.0$ (dashed lines). The mixed layer is between the vertical dashed lines.

$=0$, we use the even symmetry conditions $\phi(0)=1$ and $D\phi(0)=0$, as the even mode is always more unstable than the odd.

Since the flow is symmetric with respect to the channel centerline, we restrict our attention to the upper half channel. Fluid 2 occupies the region $0\leqslant y\leqslant p$. Fluid 1 lies between $p+q\leqslant y\leqslant 1$. The region $p\leqslant y\leqslant p+q$ contains mixed fluid. The viscosity is described by a steady function of y, scaled by the inner fluid viscosity μ_2,

$$\mu(y)=1 \quad \text{for} \quad 0\leqslant y\leqslant p, \tag{3}$$

$$\mu(y)=1+(m-1)\xi^3[10-15\xi+6\xi^2], \quad 0\leqslant\xi\leqslant 1, \tag{4}$$

$$\mu(y)=m \quad \text{for} \quad p+q\leqslant y\leqslant 1. \tag{5}$$

Here $\xi\equiv(y-p)/q$ is the mixed layer coordinate. We have assumed a fifth-order polynomial profile for the viscosity in the mixed layer, whose coefficients maintain the viscosity and its first two derivatives continuous across the mixed layer. The exact form of the profile is unimportant. For a plot of the profile $m=0.9$, see Fig. 3.

The basic flow $\bar{U}(y)$ is obtained by requiring the velocity and all relevant derivatives to be continuous at the edges of the mixed layer [10]:

$$\bar{U}(y)=1-Gy^2/2 \quad \text{for} \quad y\leqslant p, \tag{6}$$

$$\bar{U}(y)=U(p)-G\int_p^y dy \; y/\mu \quad \text{for} \quad p\leqslant y\leqslant p+q, \tag{7}$$

$$\bar{U}(y)=G(1-y^2)/2m \quad \text{for} \quad y\geqslant p+q. \tag{8}$$

Here G is the streamwise pressure gradient.

It can be seen, comparing the mean profile $\bar{U}(y)$ to that of the neat fluid (cf. Fig. 3), that nothing dramatic happens to

this profile even when the mixed layer is chosen to overlap a typical critical layer. Accordingly, we need to look for the origin of the large effect of Fig. 2 in the energetics of the disturbances. To do so, recall that the streamwise and normal components of the disturbance velocity $\hat{u}_p(x,y,t)$ and $\hat{v}_p(x,y,t)$ may be expressed via stream function as usual: $\hat{u}_p(x,y,t)=\partial\hat{\phi}_p/\partial y$ and $\hat{v}_p(x,y,t)=-\partial\hat{\phi}_p/\partial x$. These functions may be written in terms of complex envelopes similar to Eq. (1),

$$\hat{u}_p(x,y,t)= \tfrac{1}{2}\{u_p(y)\exp[ik_p(x-c_pt)]+\text{c.c.}\}\exp(\gamma_pt), \tag{9}$$

$$\hat{v}_p(x,y,t)= \tfrac{1}{2}\{v_p(y)\exp[ik_p(x-c_pt)]+\text{c.c.}\}\exp(\gamma_pt). $$

The pressure disturbance $\hat{p}_p$ is defined similarly.

Define now a disturbance of the density of the kinetic energy of the primary instability

$$\hat{E}_p(x,y,t)= \tfrac{1}{2}[\hat{u}_p(x,y,t)^2+\hat{v}_p(x,y,t)^2]. \tag{10}$$

We can express the mean (over x) density of the kinetic energy as follows:

$$E_p(y,t)\equiv\langle\hat{E}_p(x,y,t)\rangle_x=\mathcal{E}_p(y)\exp(2\gamma_pt),$$
$$\mathcal{E}_p(y)= \tfrac{1}{4}(|u_p(y)|^2+|v_p(y)|^2). \tag{11}$$

The physics of our phenomenon will be discussed in terms of the balance equation for the averaged disturbance kinetic energy. Starting from the linearized Navier-Stokes equations for $\hat{u}_p$ and $\hat{v}_p$, dotting it with the disturbance velocity vector, averaging over one cycle in x and using Eqs. (9)–(11) leads to

$$2\gamma_p\mathcal{E}_p(y)=\nabla\cdot J_p(y)+W_{p+}(y)-W_{p-}(y), \tag{12}$$

where the energy flux $J_p(y)$ in the y direction, rates of energy production (energy taken up by the primary instability from the mean flow) $W_{p+}(y)$ and energy dissipation (by the viscosity) $W_{p-}(y)$ are given by

$$J_p(y)\equiv\frac{[u_p(y)p_p^*(y)+\text{c.c.}]}{4\rho}+\frac{1}{\text{Re}}\mu(y)\nabla\mathcal{E}_p(y), \tag{13}$$

$$W_{p+}(y)\equiv-\frac{1}{4}D\bar{U}(y)[u_p(y)v_p^*(y)+\text{c.c.}], \tag{14}$$

$$W_{p-}(y)\equiv\frac{\mu(y)}{\text{Re}}\left\{2k_p^2\mathcal{E}_p(y)+\frac{1}{2}[|Du_p(y)|^2+|Dv_p(y)|^2]\right\}.$$

The superscript * denotes complex conjugate. To plot these functions we need to solve Eq. (2) as an eigenvalue problem, to obtain c_p, γ_p, and $\phi_p(y)$ at given Re and k_p. The value
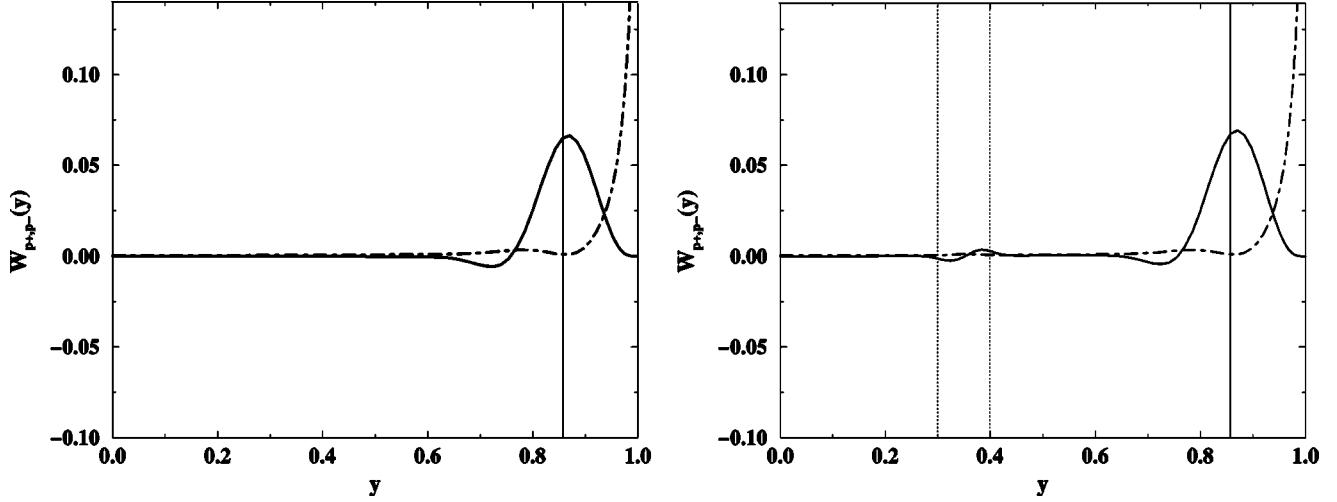
FIG. 4. Energy balance, production $W_{p+}(y)$, solid line; dissipation $W_{p-}(y)$, dot-dashed line, Re$=5772$. Left, $m=1$, $\Gamma_{p+}=\Gamma_{p-}=0.0148$. Right, $m=0.9$, $p=0.3$, $\Gamma_{p+}=0.0158$, $\Gamma_{p-}=0.0148$. In this figure and in the two subsequent figures the solid vertical lines show the location y_c of the critical lines, whereas the region between the dotted lines is the mixed layer.

of c_p determines the position of the critical layer. It is convenient to compute and compare the space averaged production and dissipation terms Γ_{p+} and Γ_{p-} defined by

$$\Gamma_{p\pm} \equiv \int_0^1 W_{p\pm}(y)dy \bigg/ \int_0^1 \mathcal{E}_p(y)dy. \qquad (15)$$

The local production of energy can be positive or negative, indicative of energy transfer from the mean flow to the primary disturbance and vice versa, respectively. The production in one region (where $W_{p+}(y)>0$) can be partly canceled out by a "counterproduction" in other region (where $W_{p+}(y)<0$).

The use of these measures can be exemplified by the neat fluid ($m=1.0$ here). The laminar flow displays its first linear instability at a threshold Reynolds number of Re$_{\text{th}}=5772$, which means that the total production Γ_{p+} across the layer becomes equal to the total dissipation Γ_{p-} at this value of Re. Examining Fig. 4, we can see that the disturbance kinetic energy is produced predominantly within the critical layer, where the basic flow velocity is close to the phase speed of the disturbance, while most of the dissipation is in the wall layer. The balance is not changed significantly when the viscosity ratio is changed to 0.9 so long as the mixed layer is not close to the critical layer. There is a small region of production and one of counter production within the mixed layer, whose effects cancel out, leaving the system close to marginal stability.

We now turn our attention to Fig. 5, in which our main point is demonstrated. The Reynolds number is the same as before, but the mixed layer has been moved close to the critical layer. It is immediately obvious that the earlier balance is destroyed. The counterproduction peak in the mixed layer is much larger than before, making the flow more stable. The wave number used is that at which the flow is least stable for the given Reynolds number at this p. For $m=0.9$, the threshold Reynolds number is 46 400. Figure 6

shows the energy balances at marginal stability—the picture is qualitatively the same here as at Re≈ 5772 for the neat fluid.

B. The mechanism of stabilization

The main factor determining the instability is the energy intake from the mean flow, which is driven by the phase change caused by the viscosity stratification. The dissipation on the other hand depends only on Reynolds number and does not respond disproportionately to changes in viscosity. We will show below [cf. Eqs. (19) and (20)] that in neat fluids, the term containing $D^2\bar{U}(y)$ in Eq. (2) is always much smaller than the important terms that govern the equations in the critical layer. However, with the introduction of a viscosity gradient within the critical layer, the gradients of the basic velocity profile will scale according to the mixed-layer coor-
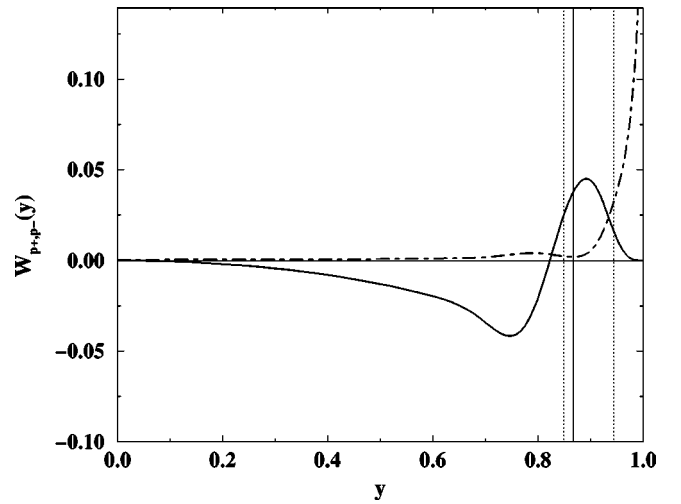

FIG. 5. Energy balance, production $W_{p+}(y)$, solid line; dissipation $W_{p-}(y)$, dot-dashed line. Re$=5772$, $m=0.9$, $p=0.85$, $\Gamma_{p+}=-0.0114$, $\Gamma_{p-}=0.0122$.
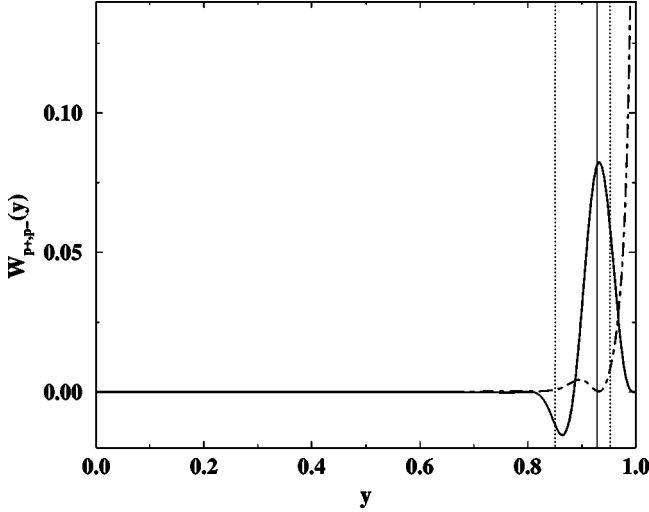
FIG. 6. Energy balance, production $W_{p+}(y)$, solid line; dissipation $W_{p-}(y)$, dot-dashed line. Re$=46400$, $m=0.9$, $p=0.85$, $\Gamma_{p+}=\Gamma_{p-}=0.0053$.

dinate ξ. We show in the analysis that follows that for $q \lesssim O(\text{Re}^{-1/3})$, the term containing $D^2\bar{U}$ is now among the most dominant. Since most of the production of disturbance kinetic energy takes place within the critical layer, we return to Eq. (2) and isolate all lowest-order effects within the critical layer. The relevant normal coordinate in the critical layer is

$$\eta \equiv \frac{y - y_c}{\epsilon}, \qquad (16)$$

where y_c is the critical point defined by $U(y_c)=c$, and ϵ is the critical layer thickness, which is a small parameter at large Reynolds number. The basic channel flow velocity may be expanded in the vicinity of the critical point as

$$U(y) = c + (y - y_c)DU(y_c) + \frac{(y - y_c)^2}{2!}D^2U(y_c) + \cdots. \qquad (17)$$

We use Eq. (17), and redefine $\phi_p(y) \equiv \Phi(\eta)$ and $\mu(y) \equiv \nu(\xi)$, to rewrite Eq. (2) within the critical layer. We obtain

$$\epsilon \sim \text{Re}^{-1/3} \equiv (k_p\text{Re})^{-1/3}, \qquad (18)$$

and the lowest-order equation in the critical layer,

$$i\eta \frac{dU}{dy}\bigg|_c D^2\Phi - \frac{iGp}{\nu^2}\chi D\nu\Phi = \nu D^4\Phi + 2\chi D\nu D^3\Phi$$
$$+ \chi^2 D^2\nu D^2\Phi, \qquad (19)$$

where $\chi \equiv \epsilon/q$ is $O(1)$ for the mixed layer. In the absence of a viscosity gradient in the critical layer (i.e., $\nu=1$), Eq. (19) would reduce to

$$i\eta \frac{dU}{dy}\bigg|_c D^2\Phi = D^4\Phi, \qquad (20)$$

which is the traditional lowest-order critical layer equation for a parallel shear flow [8]. The mechanism for the stabilization now begins to be apparent: there are several new terms which can upset the traditional balance between inertial and viscous forces. In order to narrow down the search further, we resort to numerical experimentation, because although all terms in Eq. (19) are estimated to be of $O(1)$, their numerical contributions are different. It transpires that the second term on the left hand side of Eq. (19) is particularly responsible; first, it is straightforward to verify that it originates from the term containing $D^2\bar{U}(y)$ in the modified Orr-Sommerfeld equation. As testimony, note the dramatic effect on $D^2\bar{U}$ in Fig. 3. Second, this term dominates the energy intake from the mean flow to the disturbance. Any reasonable viscosity gradient of the right sign is seen to pick up this term, leading to a vastly enhanced stability. On the other hand all the terms on the rhs of Eq. (19) contribute only to dissipation.

Indeed, in the light of this discussion, we can expect that the large effect of retardation of the instability would even increase if we make the mixed layer thinner. This is indeed so. Nevertheless, one cannot conclude that instability can be retarded at will, since other disturbances, differing from the primary mode, become unstable first, albeit at a much higher Reynolds number than the primary mode; when we stabilize a given mode substantially, we should watch out for other preexisting and newly destabilized modes which may now be the least stable.

Finally, we connect our findings to the phenomenon of drag reduction in turbulent flows. Since the total dissipation can be computed just from the knowledge of the velocity profile at the walls, any amount of drag reduction must be reflected by a corresponding reduction of the gradient at the walls. Concurrently, the energy intake by the fluctuations from the mean flow should reduce as well. Indeed, the latter effect was measured in both experiments [11] and simulations [12,13]. The question is which is the chicken and which is the egg. In our calculation we identified that the reduction in production comes first. From Figs. 4 and 5 that are at the same value of Re, we see that the dissipation does not change at all when the mixed layer moves, but the production is strongly affected. Of course, at steady state, the velocity gradient at the wall must adjust as shown in Fig. 6.

C. Continuous viscosity profile

One could think that the strong stabilization discussed in the preceding subsection is only due to the precise positioning of the mixed layer at the critical layer. If so, the result would have very little generic consequence. In this subsection we show that any reasonable viscosity profile achieves the same effects. We do not attempt here to "optimize" the viscosity profile to achieve larger stabilization. Our concern is with the point of principle, i.e., that *any* viscosity profile in the critical layer, in which the viscosity reduces towards the wall would lead to stabilization. As a physical example, we consider the effective viscosity profile reported in Ref. [7] (in
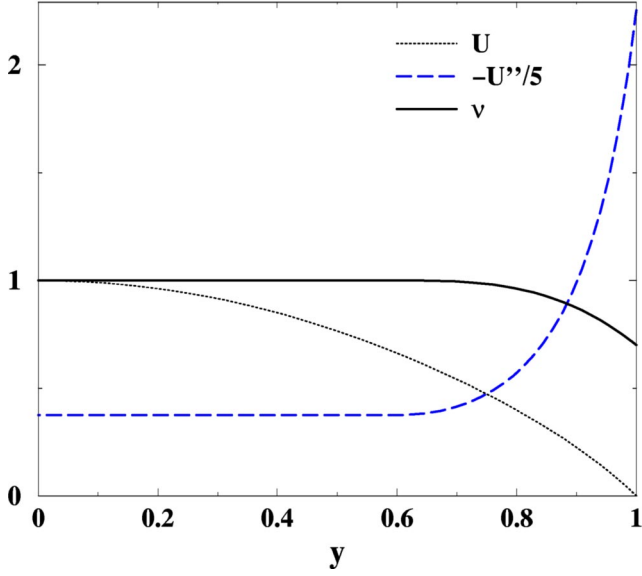
FIG. 7. Prescribed continuous viscosity profile (in accordance with that obtained in direct numerical simulations of polymeric flow). The corresponding laminar velocity profile $\bar{U}(y)$ and its second derivative are also shown.

their Fig. 5) which is obtained from simulations of a turbulent channel flow with polymer additive. It may be prescribed as

$$\mu(y) = 1 \quad \text{for} \quad 0 \leqslant y \leqslant p, \tag{21}$$

$$\mu(y) = 1 + (m-1)\left(\frac{y-p}{q}\right)^3, \tag{22}$$

with $q \sim 0.4$ and $m \sim 0.7$, as shown in Fig. 7. The energy balance for the least stable primary mode at Re$=5772$ for this case (Fig. 8) shows a large counter production of disturbance kinetic energy, which is in fact more pronounced than what we obtained with a mixed layer (Fig. 5). Thus the
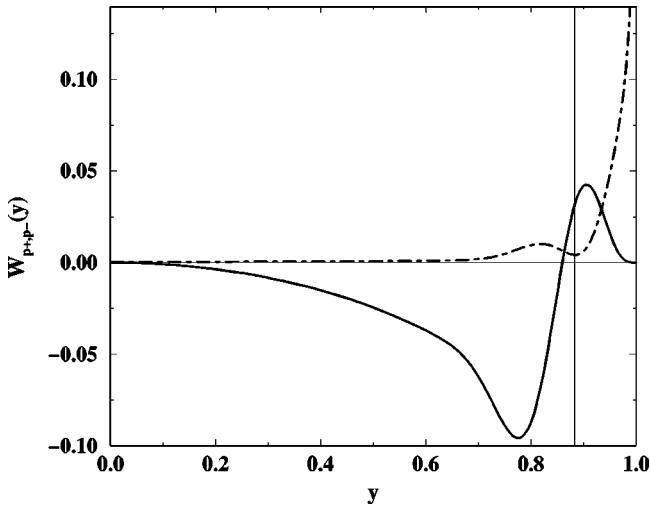
FIG. 8. Energy balance, production $W_{p+}(y)$, solid line; dissipation $W_{p-}(y)$, dot-dashed line. Re$=5772$, $m=0.7$, $p=0.6$, $q=0.4$, $\Gamma_{p+}=-0.0345$, $\Gamma_{p-}=0.0138$.

strong stabilization effect does not require careful placing of the viscosity variation at a particular layer. It is sufficient that there exists a viscosity variation in the region of the critical layer (indicated as the vertical line in Fig. 8) to achieve the stabilization. The reader should note that in our example we insert the viscosity profile by hand. This differs from other stability studies of the full viscoelastic equations for a non-Newtonian fluid where the viscoelastic profiles, if they exist, should appear naturally [14].

It comes as no surprise that this continuous viscosity profile behaves very similarly to the thin mixed layer. If we return to Eq. (19), we will see that all we have now done is to increase both $D\nu$ (which is proportional to $m-1$) and q threefold (the effective q here is closer to 0.3 than 0.4, as we can see from Fig. 7), so the ratio remains the same.

III. SECONDARY INSTABILITIES

A laminar flow through a channel is linearly unstable at Re$=5772$. In all except the cleanest experiments, however, the flow becomes turbulent at much lower Reynolds numbers, as low as 1000 [15,16]. This is because the linear stability analysis is carried out on a steady laminar velocity profile, whereas a real flow, except under carefully designed clean conditions, consists in addition of small but finite disturbances (most of whom will decay at long times). The stability behavior of the real flow is quite different from that of the steady profile: the actual flow is unstable to new modes, often referred to as secondary modes. The secondary modes are often three dimensional, and their signature is prominent in fully developed turbulence. As described below, the secondary instabilities are studied by a Floquet analysis of the periodic primary flow we obtained earlier.

As usual in the analysis of secondary instabilities [17,18], we begin by splitting the flow into a periodic component (consisting of the mean laminar profile in addition to the primary wave) and a secondary disturbance, e.g.,

$$U_{\text{total}}(x,y,z,t) = U(x,y,t) + u_s(x,y,z,t), \tag{23}$$

where

$$U(x,y,t) = \bar{U}(y)\hat{x} + A_p(t)\{[u_p(y)\hat{x} + v_p(y)\hat{y}]$$
$$\times \exp[ik_p(x - c_p t)] + \text{c.c.}\}. \tag{24}$$

Here $\hat{x}$ and $\hat{y}$ are unit vectors in x (steamwise) and y (wall normal) directions. The amplitude A_p of the primary disturbance changes very slowly with time, and dA_p/dt may be neglected during one time period. The spatial and temporal dependence of the secondary disturbance is written in the form

$$u_s(y,r_\perp,t) \equiv \text{Re}\{u_{s+}(y)\exp[i(k_+ \cdot r_\perp - \omega_+ t)]$$
$$+ u_{s-}(y)\exp[i(k_- \cdot r_\perp - \omega_- t)]\}, \tag{25}$$

where $r_\perp \equiv x\hat{x} + z\hat{z}$, and $k_\pm = k_\pm \hat{x} \pm k_z \hat{z}$. We substitute the above ansatz into the Navier-Stokes and continuity equa-

tions, and retain linear terms in the secondary disturbance. On averaging over x, z, and t, only the resonant modes survive, which are related by

$$\mathbf{k}_+ + \mathbf{k}_- = k_p \hat{\mathbf{x}}, \quad \text{therefore} \quad \mathbf{k}_\pm = \pm \mathbf{q} + \frac{k_p}{2} \hat{\mathbf{x}}, \quad (26)$$

for any vector $\mathbf{q}$, and

$$\omega_+ = \omega + i\gamma \quad \text{and} \quad \omega_- = (\omega_p - \omega) + i\gamma. \quad (27)$$

Eliminating the disturbance pressure and streamwise component of the velocity, we get the equations for the secondary disturbances v_s and w_s. Using the notation $f_\pm \equiv -iw_{s\pm}/k_z$, the equations read [19]

$$[i(\omega_+ - k_+ U) + \nu(D^2 - k_+^2 - k_z^2) + (D\nu)D]$$

$$\times [(k_+^2 + k_z^2)f_+ - Dv_+] - ik_+ DUv_+ - \frac{A_p k_+}{2k_-}\{[ik_+ u_p D$$

$$+ v_p D^2 + ik_- Du_p]v_-^* + [(k_z^2 - k_- k_+)v_p D$$

$$+ ik_+ (k_-^2 + k_z^2)u_p]f_-^*\} = 0 \quad (28)$$

and

$$[i(\omega_+ - k_+ U) + \nu(D^2 - k_+^2 - k_z^2) + (D\nu)D](Df_+ - v_+)$$

$$+ [-ik_+(DU) + (D^2 \nu)D + (D\nu)(D^2 - k_+^2 - k_z^2)]f_+$$

$$+ \frac{A_p(k_p + k_-)}{2}\left[iu_p(v_-^* + Df_-^*) - \frac{v_p}{k_-}Dv_-^*\right]$$

$$+ \frac{A_p}{2}\left[v_p\left(\frac{k_p k_z^2}{k_-} + D^2\right) - ik_-(Du_p)\right]f_-^* = 0, \quad (29)$$

The boundary conditions are

$$\mathbf{u}_s = 0 \quad \text{at} \quad y = \pm 1. \quad (30)$$

Equations (28) and (29), along with two corresponding equations in v_-^* and f_-^*, describe an eigenvalue problem for the secondary instability. The four equations are solved by a Chebychev collocation spectral method, details of the solution procedure are available in Ref. [19]. The computations have been conducted on a half channel on grounds of symmetry. Both varicose and sinuous modes have been tried, and the more unstable of the two, i.e., the modes varicose in v_+ and v_- have been used. Simulations on a full channel show that the most unstable modes could have v_+ and v_- different at the centerline. However, the difference with present results of the growth rates would be small.

The most unstable secondary mode in our case is found to be the subharmonic, for which $\mathbf{q} = k_z \hat{\mathbf{z}}$. The production and dissipation are computed as before.

We survey in turn the thin mixed-layer profile, and the continuous viscosity profile to see what the viscosity variation does to the secondary instability.
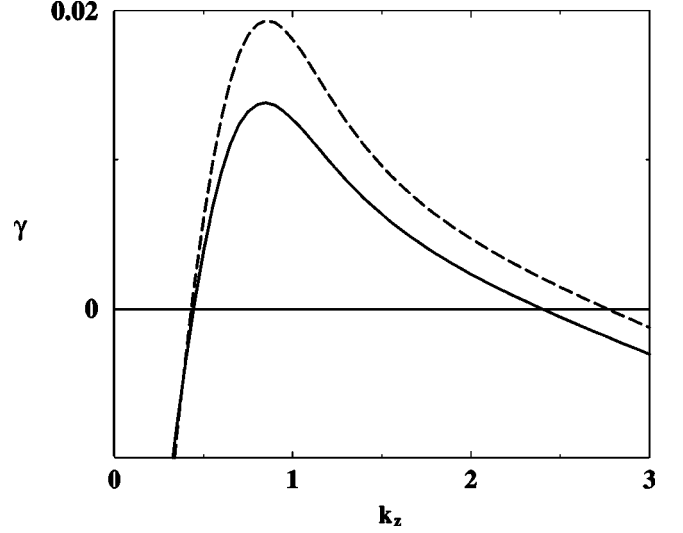

FIG. 9. Dependence of growth rate on spanwise wave number. Solid line, varying viscosity ($p=0.8, q=0.1, m=0.9$); dashed line, constant viscosity ($m=1$). $k_p=1, A_p=0.005, \text{Re}=6000$.

A. Mixed layer

The velocity and viscosity profiles here are as given in Fig. 3, and the primary instability is that presented in Sec. II A. Since the subharmonic ($k_+ = k_- = k_p/2$) is the least stable mode, we present this case alone. In Fig. 9 a typical dependence of the growth rate of the secondary mode on the spanwise wave number is shown. We can see that the viscosity variation damps the secondary mode significantly, but it is still unstable. However, there is a crucial difference in the *primary* instabilities of the two: the primary is unstable for a constant viscosity flow, but very stable in the mixed-layer case. Therefore at long times, the secondary mode, which feeds on the primary for its existence, dies down in the latter case. To compute the time dependence of the amplitude of the secondary mode, we computed the growth rate γ by neglecting the time dependence of the amplitude of the primary modes. As a result we obtain the growth rate $\gamma[A_p(t)]$, in which $A_p(t)$ can be an exponentially growing or a decaying function of time. Having this growth rate we can present the time dependence of the amplitude of the secondary mode, see Fig. 10. Without the viscosity contrast, the amplitude of the secondary mode increases (essentially exponentially). With the viscosity contrast the amplitude decays in time.

We now observe the balances of energy initially and at a later time in Figs. 11 and 12, respectively. The initial balance of energy is not so different from the constant viscosity case. At the later time, however, the production of secondary kinetic energy is significantly lower. The location y_c of the critical point is seen from the figures to be close to the layer of stratified viscosity. If the two were well separated, the stratification would do nothing to the secondary mode.

A lowest-order analysis of the secondary stability equations is not as straightforward as for the primary mode, since the secondary is highly dependent on the amplitude of the primary [19]. We may, however, make the following observations from a critical layer analysis of Eqs. (28) and (29)
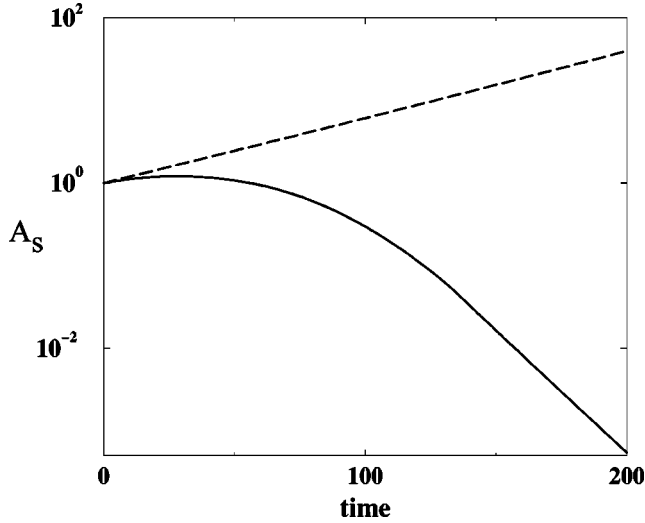
FIG. 10. Amplitude of the secondary mode in logarithmic scale as a function of time. Dashed line, constant viscosity, $m=1$. Here $\gamma_p=0.0003$, and the primary mode is unstable. Solid line, varying viscosity; here $\gamma_p=-0.0206$, the primary mode is stable. All conditions are like in Fig. 9, in particular, $A_p(t=0)=0.005$.

and their counterparts. When $A_p \gg \epsilon$, [cf. Eq. (18)] only the nonlinear terms appear at the lowest order, and the secondary mode is completely driven by the primary. When $A_p \sim O(\epsilon)$, both the basic terms and the nonlinear terms contribute at the lowest order. It may be numerically determined, however, that the secondary is slaved to the primary here as well. When $A_p=o(\epsilon)$, the lowest-order theory for the secondary is (not surprisingly) exactly that given by Eq. (19) for the primary.

A direct estimate of the effect of the viscosity stratification on the secondary mode is obtained from the threshold amplitude A_{th} of the primary for the instability. At a Rey-
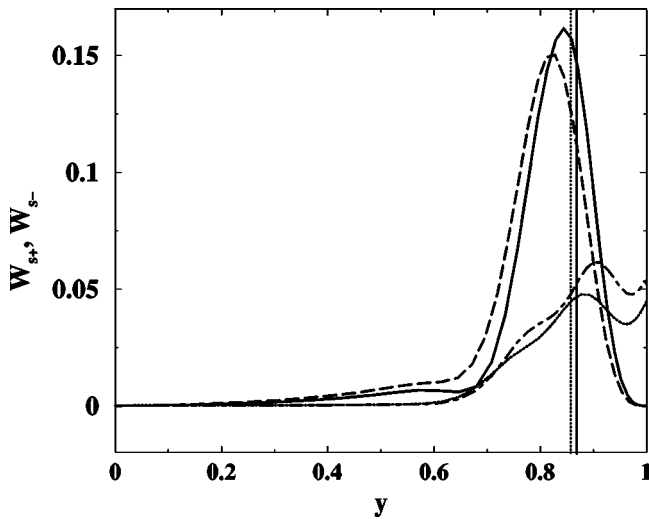

FIG. 11. Production W_{s+} and dissipation W_{s-} of the kinetic energy of the secondary disturbance at time=0. Solid line, $W_{s+}, m=0.9$; dot-dashed line, $W_{s-}, m=0.9$; long dashes, $W_{s+}, m=1$; dotted line, $W_{s-}, m=1$. The vertical lines show y_c (the critical point location) for $m=0.9$ (solid) and $m=1$ (dotted).
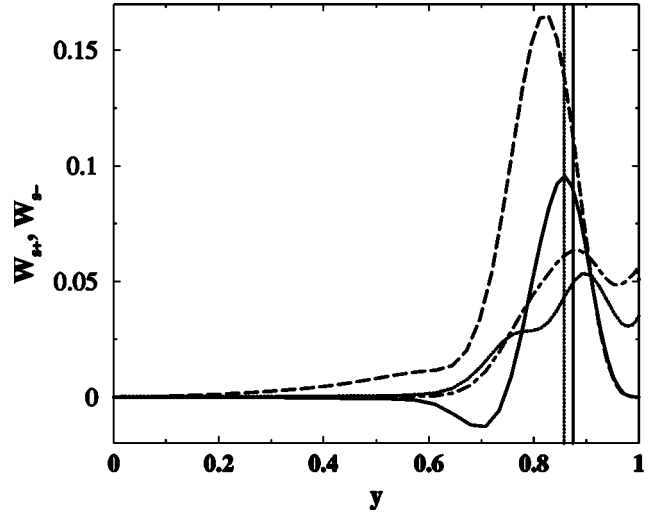

FIG. 12. Production W_{s+} and dissipation W_{s-} of the kinetic energy of the secondary disturbance at time=40. Solid line, $W_{s+}, m=0.9$; dot-dashed line, $W_{s-}, m=0.9, A_p=0.002\ 15$; long dashes, $W_{s+}, m=1$; dotted line, $W_{s-}, m=1, A_p=0.005\ 06$.

nolds number of 6000 and primary wave number of $k_p=1$, for a neat fluid, all secondary modes are damped if $A_{th} < 0.002$, while for the continuous viscosity profile, all secondary modes continue to be damped even for larger primary disturbances, up to $A_{th}=0.005$. When the Reynolds number is reduced to 2000, the threshold amplitudes are 0.012 and 0.016 for the neat and viscosity-stratified fluids respectively.

B. Continuous viscosity profile

The velocity and viscosity profiles here are as given in Fig. 7, and the primary instability is that presented in Sec. II C. The counterparts for the continuous viscosity profile of Figs. 9–12 are presented in Figs. 13–16, respectively. It is clear that nothing has changed qualitatively.

Figure 17 shows the dependence of the growth rate of the secondary mode on the amplitude of the primary disturbance.
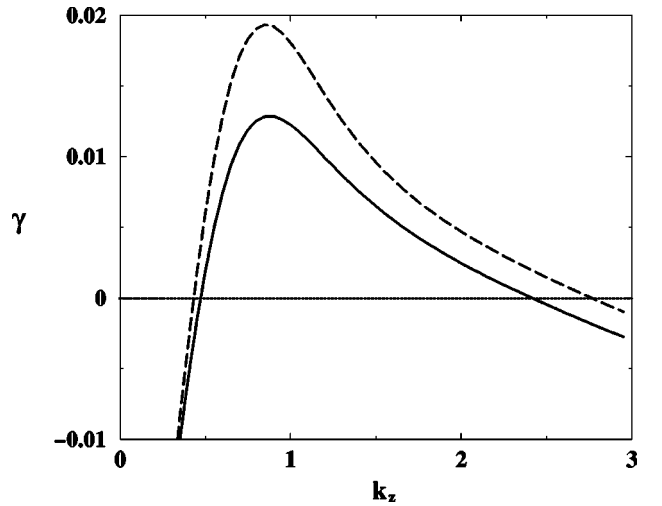

FIG. 13. Dependence of growth rate on spanwise wave number. Solid line, varying viscosity [according to Eq. (22)]; dashed line, constant viscosity. Wave numbers and Re as in Fig. 9.
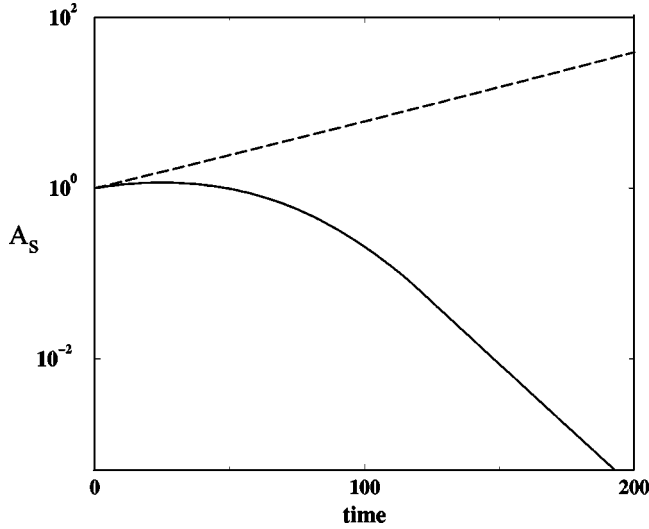
FIG. 14. Variation of the amplitude of the secondary instability mode with time. Solid line, varying viscosity, $\gamma_p = -0.0244$; dashed line, constant viscosity, $\gamma_p = 0.0003$. Wave numbers and Re as in Fig. 10.

It is clear that the instability is reduced by the stratification of viscosity, but there is no dramatic effect in the secondary instability alone. We may conclude that the large effect comes from the complete reliance of the secondary disturbance on the primary. To make this point clearer, we investigated a situation in which the primary disturbance is stable. This is the case for example, when $R = 3000$. The results for this Reynolds number are shown in Figs. 18 and 19. These are similar to Figs. 13 and 14 above, except that the primary disturbance is stable for both constant and varying viscosities. Accordingly, the disturbances die out at long times. Note that in the case of a constant viscosity, there is more time for nonlinearities to act, and the transition to turbulence is more likely.
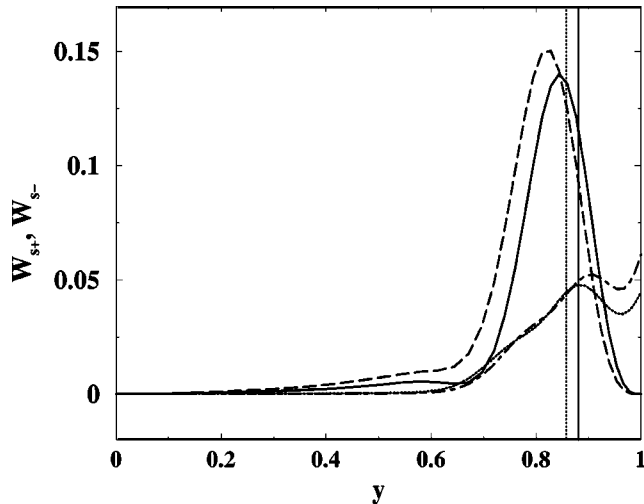

FIG. 15. Production and dissipation at time=0. Solid line, varying viscosity; dashed line, constant viscosity, $A_p = 0.005$ for both.
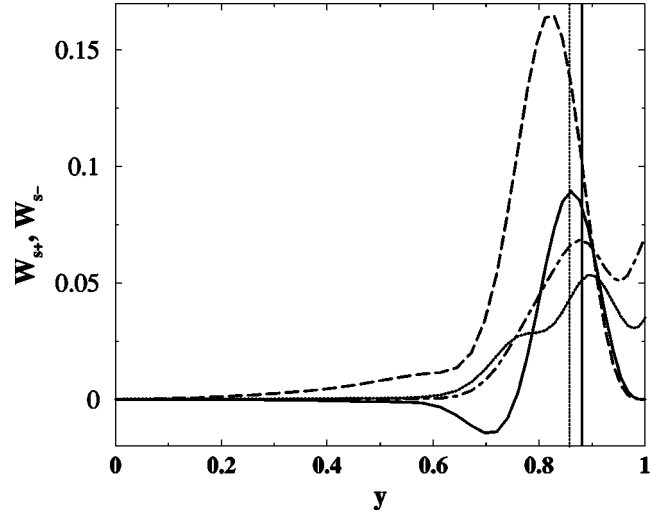

FIG. 16. Production and dissipation at time=40. Solid line, varying viscosity, $A_p = 0.001\,84$; dashed line, constant viscosity, $A_p = 0.005\,06$.

IV. CONCLUDING REMARKS

We addressed the primary and secondary instability of simple channel flows, and examined the effects of small viscosity variations. We find dramatic effects of stabilization when the viscosity variations exist in the vicinity of the critical layers, in which the speed of propagation of the modes coincided with the mean velocity of the basic flow. With about 10% viscosity changes we can have very large increases in the threshold Reynolds numbers for instability. In all cases we find that the main mechanism for the large effects is the reduction of the intake of energy from the mean flow to the putative unstable modes, which therefore become stable. For the same Reynolds numbers in Newtonian fluids there is no such mechanism for stabilization, and these flows will become turbulent. We would like to propose that similar
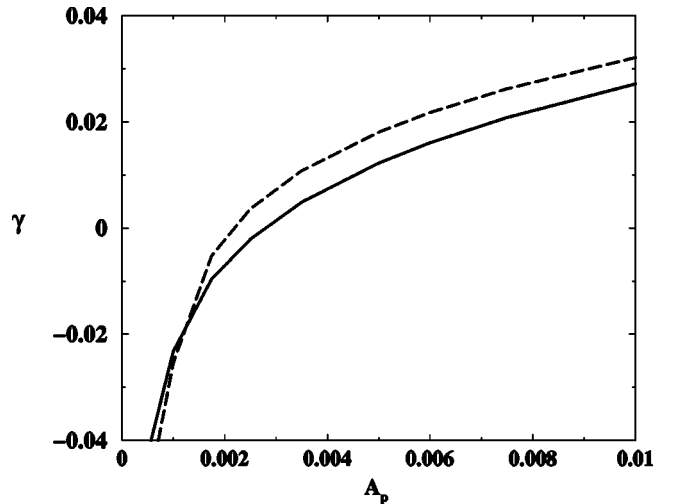

FIG. 17. Dependence of growth rate of the secondary mode on the amplitude of the primary disturbance. Solid line, stratified viscosity; dashed line, constant viscosity. $k_p = 1$, $k_+ = 0.5$, $k_z = 1$, Re $= 6000$.
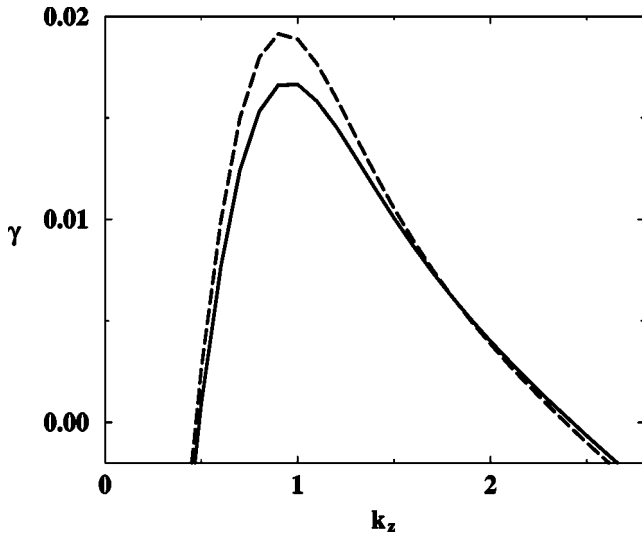
FIG. 18. Dependence of growth rate on spanwise wave number. Solid line, varying viscosity, dashed line, constant viscosity. $k_p = 1$, $A_p = 0.02$, Re=3000.
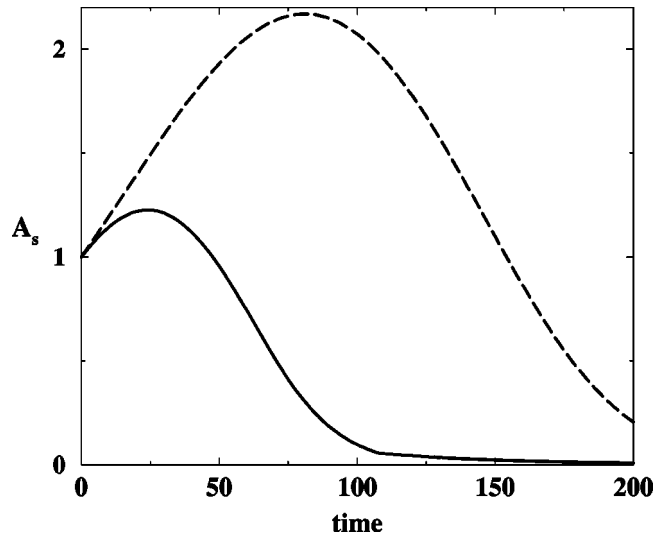

FIG. 19. Amplitude of the secondary mode as a function of time. Solid line, varying viscosity, dashed line, constant viscosity; all conditions are like Fig. 18, in particular, $A_p(t=0) = 0.02$.

effects should be examined in the case of turbulent drag reduction by polymer additives.

We recognize that in a turbulent flow there are many more modes that interact, but we propose that as here, it is the energy budget (specifically the energy intake from the mean flow) of the energy containing modes that will change due to the existence of a space-dependent effective viscosity. In fact, this view is born out by recent direct numerical simulations of the FENE-P model equations, cf. Ref. [20]. The advantage of the present calculation is that we can consider explicitly all the putative unstable modes, and conclude that with a viscosity gradient similar to that seen in polymeric turbulent flows the linear threshold Re_{th} goes up five times (to 31 000). We note in passing that this effect had not been put to an experimental test, and it would be exciting to have a confirmation of our predictions by future experiments. For actual turbulent flows, we will need first to identify what are the main modes that interact between themselves and with the mean flow. A significant numerical effort is required, but appears worthwhile due to the importance of the phenomenon of drag reduction, and its relative lack of understanding.

We have demonstrated that the exact form of the viscosity profile is immaterial; a continuous profile of viscosity in the critical region behaves exactly like a thin mixed layer. We have shown that the secondary three-dimensional modes of instability are ''slaved'' to the primary linear mode of instability: the mechanism which stabilizes the primary mode indirectly ensures that the secondary is damped out quickly.

Finally we note that a linear disturbance can rear its head either in the form of the fastest growing (or slowest decaying) mode as considered here; or in a nonmodal form with a transient growth followed by long-term decay [21]. The former situation will correspond to relatively high Reynolds numbers, or cleaner setups. We expect similar conclusions in the latter situation as well.

[1] R.H. Nadolink and W.W. Haigh, ASME Appl. Mech. Rev. **48**, 351 (1995).

[2] J.L. Lumley, Annu. Rev. Fluid Mech. **1**, 367 (1969).

[3] K.R. Sreenivasan and C.M. White, J. Catal. **409**, 149 (2000).

[4] M. Tabor and P.G. de Gennes, Europhys. Lett. **2**, 519 (1986).

[5] P.G. de Gennes, *Introduction to Polymer Dynamics* (Cambridge University Press, Cambridge, 1990).

[6] R. Govindarajan, V.S. L'vov, and I. Procaccia, Phys. Rev. Lett. **87**, 174501 (2001).

[7] R. Sureshkumar, A.N. Beris, and R.A. Handler, Phys. Fluids **9**, 743 (1997).

[8] C.C. Lin, Q. Appl. Math. **3**, 117 (1945).

[9] F.M White, *Viscous Fluid Flow* (McGraw-Hill, New York, 1991).

[10] B.T. Ranganathan and R. Govindarajan, Phys. Fluids **13**, 1 (2001).

[11] J.M. J den Toonder, M.A. Hulsen, G.D.C Kuiken, and F.T.M Niewstadt, J. Fluid Mech. **337**, 193 (1997).

[12] C.D. Dimitropoulos, R. Sureshkumar, A.N. Beris, and R.A. Handler, Phys. Fluids **13**, 1016 (2001).

[13] E. De Angelis, Ph.D. thesis, Università di Roma, La Sapienza, 2000.

[14] H.K. Wilson and J.M. Rallison, J. Non-Newtonian Fluid Mech. **85**, 273 (1999).

[15] S.A. Orszag and L.C. Kells, J. Fluid Mech. **96**, 159 (1980).

[16] L.N. Trefethen, A.E. Trefethen, S.C. Reddy, and T.A. Driscoll, Science **261**, 578 (1993).

[17] T. Herbert, Annu. Rev. Fluid Mech. **20**, 487 (1988).

[18] T. Herbert, Phys. Fluids **26**, 871 (1983).

[19] A. Sameen and R. Govindarajan (unpublished).

[20] E. De Angelis, C.M. Casciola, V.S. L'vov, R. Piva, and I. Procaccia, Phys. Rev E (to be published), e-print nlin. CD/0210064.

[21] See, for example, S.J. Chapman, J. Fluid Mech. **451**, 35 (2002).